Crack Initiation and Propagation in Circular Rubber Bearings Subjected to Cyclic Compression

Hsoung-Wei Chou,[1] Jong-Shin Huang[2]

[1]*Institute of Nuclear Energy Research, Taoyuan 32546, Taiwan*
[2]*Department of Civil Engineering, National Cheng Kung University, Tainan 70101, Taiwan*

Received 31 March 2010; accepted 22 November 2010
DOI 10.1002/app.33817
Published online 4 March 2011 in Wiley Online Library (wileyonlinelibrary.com).

ABSTRACT: The fatigue failure mechanism of rubber bearings under cyclic compression is important in evaluating their fatigue lives and thus is analyzed theoretically and numerically here. At first, the stress distributions in a bonded rubber cylinder derived from three different existing models were utilized to calculate the cracking energy densities within it. Next, the location of fatigue crack initiation and the direction of subsequent crack propagation in circular rubber bearings were consecutively determined. Furthermore, finite element numerical results were compared to those obtained theoretically from the three models to check their validity in predicting the fatigue crack initiation and propagation in circular rubber bearings. Based on the quasi-statically theoretical and numerical results, it is found that the fatigue cracks initiate first at the outermost boundary between rubber and steel plates and propagate later inwards to the center of circular rubber bearings. The corresponding fatigue failure mechanism obtained theoretically and numerically is consistent with experimental findings reported previously. © 2011 Wiley Periodicals, Inc. J Appl Polym Sci 121: 1747–1756, 2011

Key words: rubber bearing; cyclic compression; crack initiation; crack propagation

INTRODUCTION

When rubbers are used as isolators and dampers in engineering structures subjected to cyclic loading, fatigue failure is of importance and needs to be taken into account in a design of rubber components. Presumably, fatigue failure of rubbers results in the reduction of their mechanical properties. Rubber bearings composed of multiple layers of rubber and steel plate are typically utilized as vibration isolators in buildings and bridges. Fatigue failure of circular rubber bearings has been frequently observed in Taiwan, for example, due to overloaded vehicles passing through bridges or live loads acting on buildings. The degradation and fatigue failure of circular neoprene rubber bearings under cyclic compression were investigated experimentally by Chou and Huang.[1] Experimental observation on the sawcut cross sections of their specimens as shown in Figure 1 indicated that fatigue cracks initiate at the interfaces between rubber and steel plates and then propagate steadily in rubber. In some cases, the fatigue failure of rubber bearings caused by cyclic compression could lead to a catastrophic failure of buildings and bridges. Therefore, the fatigue failure mechanism of rubber bearings subjected to cyclic compression should be exploited in detail when both structural integrity and durability of buildings and bridges are sought.

The static and dynamic responses of rubber bearings mainly depend on the material properties of rubber and the ratio of the thicknesses of rubber and steel plates. For simplicity, the mechanical properties of a circular rubber bearing can be theoretically obtained by analyzing those of a bonded rubber cylinder with two steel plates separated by a rubber core. For a bonded rubber cylinder with a radius of a and a thickness of h as schematically illustrated in Figure 2, its shape factor defined as the ratio of compressed surface area to lateral free surface area is $S = a/2h$. By conducting a series of cyclic compression tests on bonded rubber cylinders with smaller shape factors, Lindley and Stevenson[2] experimentally verified that some fatigue cracks initiated on their circumferential surfaces near the outermost boundary between rubber and steel plates. At the same time, the induced circumferential cracks propagated along the direction perpendicular to edge steel plates until the bulge of rubber was separated completely from the core of each bonded rubber cylinder. Based on the assumption of two ways of crack propagation, namely internal penny-shaped cracks

Correspondence to: J.-S. Huang (jshuang@mail.ncku.edu.tw).

Contract grant sponsor: National Science Council, Taiwan, R.O.C.; contract grant number: NSC 90-2211-E006-109.

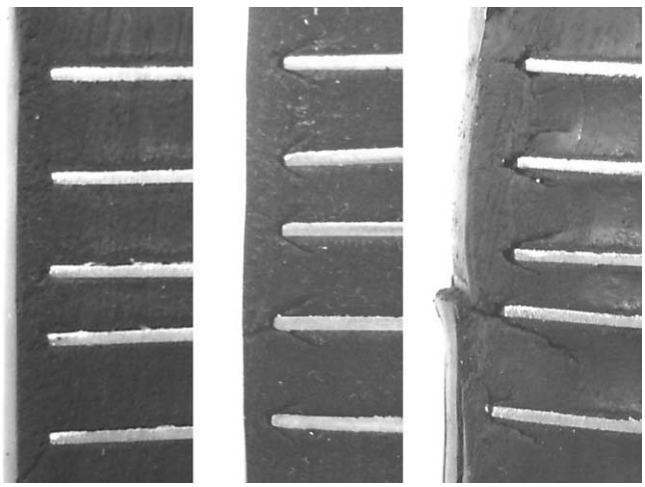

Figure 1 Photographs of the fatigue crack initiation and propagation in circular neoprene rubber bearings with a shape factor $S = 2.5$ after suffering from different cycles of compressive loading.

and external ring-shaped cracks, Leicht et al.[3,4] numerically studied the fatigue failure mechanism of bonded rubber cylinders. They further analyzed the relationship between strain energy density and crack length and then proposed a fatigue life prediction for bonded rubber cylinders with various shape factors under cyclic compression. However, the fatigue crack initiation and propagation in circular rubber bearings can not be represented thoroughly by the two assumed ways of crack propagation, limiting the application of their fatigue life prediction. Hence, the fatigue crack initiation and propagation are important and essential in evaluating the fatigue lives of rubber bearings under cyclic compression.

To describe the fatigue crack initiation and propagation in rubbery materials under multiaxial stresses, Mars[5,6] introduced a concept of cracking energy density, defined as the energy produced by the principal stresses acting directly on each preexisting crack. Mars suggested that the energy required to tear a crack or employed to determine the direction of crack propagation in rubbery materials under multiaxial stresses is cracking energy density. Also, the orientation of maximum cracking energy density is the direction of maximum principal tensile stress if there is no relatively larger preexisting crack in rubbery materials. Intrinsic flaws in rubbery materials resulting from manufacturing were observed by many researchers.[7–10] The size of intrinsic flaws plays an important role in determining the fatigue lives of rubbery materials.[11–13] Thus, the fatigue crack in rubbery materials initiates from an intrinsic flaw with the maximum cracking energy density and its crack surface is perpendicular to the direction of principal tensile stress.

Up to now, the fatigue crack initiation and propagation have been studied extensively in many rubbery components such as tires and hoses, but paid less attention in rubber bearings. In the article, we aim at quasi-statically analyzing the fatigue crack initiation and propagation in circular rubber bearings under cyclic compression. At first, the stress distributions within a bonded rubber cylinder under quasi-static compression derived from three different existing theoretical models will be utilized to calculate the cracking energy densities within it. Then, the location of fatigue crack initiation and the direction of subsequent crack propagation in circular rubber bearings with different shape factors will be theoretically determined. In addition, the fatigue crack initiation and propagation in circular rubber bearings can be numerically studied by using finite element analyses (FEA). Consequently, FEA numerical results are compared to those obtained from the three theoretical models to check their applicability and validity in predicting the fatigue crack initiation and propagation in bonded rubber bearings under cyclic compression.

THEORETICAL ANALYSIS

The cracking energy density W_C around a crack in rubber under multiaxial stresses as shown in Figure 3 can be calculated as following:[5,6]

$$W_C = \hat{r}^T \kappa^T \left[\int_0^{\bar{\varepsilon}} \bar{\sigma} d\bar{\varepsilon} \right] \kappa \hat{r} \tag{1}$$

where $\hat{r}$ is a unit vector normal to the crack surface plane, κ is the transformation matrix from the crack surface plane to the principal stresses plane, and $\bar{\sigma}$ and $\bar{\varepsilon}$ are the induced principal stresses and strains acting around the crack due to external multiaxial stresses. Three assumptions are made in analyzing

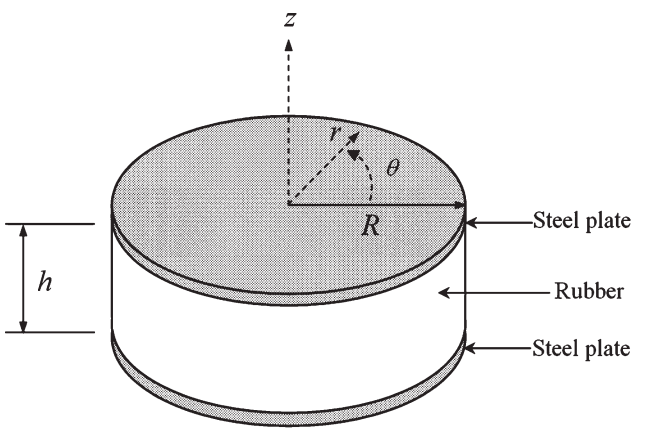

Figure 2 A bonded rubber cylinder with a radius of a and a height of h in the $r - \theta - z$ cylindrical coordinate.

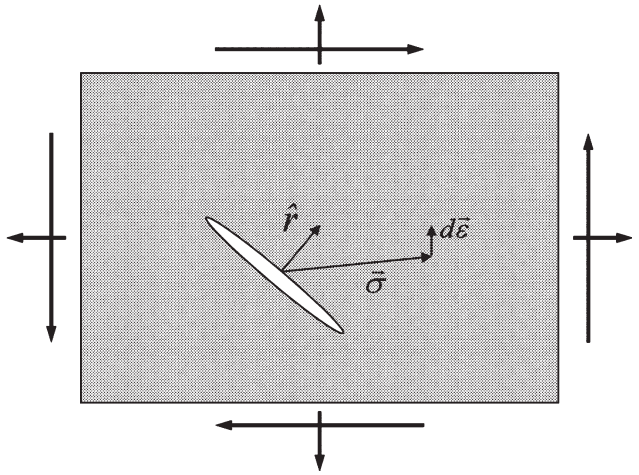

Figure 3 Crack surface normal vector $\hat{r}$, stress vector $\vec{\sigma}$, and strain increment vector $d\vec{\varepsilon}$ used for calculating the cracking energy density of a pre-existing crack.

quasi-statically the fatigue crack initiation and propagation in bonded rubber cylinders. At first, intrinsic flaws with a uniform size distribute randomly in rubber; in other words, no intrinsic flaws are large enough to affect the crack propagation in bonded rubber cylinders. Hence, isotropy and small deformation of rubber are considered here. Second, the stress distribution in rubber still remains the same when the crack grows steadily. That is, the fatigue crack is relatively small as compared to the dimension of bonded rubber cylinders and thus the effect of crack propagation on the stress field of bonded rubber cylinders is negligible. Third, principal tensile stress dominates the crack propagation in rubber. The minimum strain energy density method,[14] which implies that the crack will propagate toward the point of minimum strain energy density around the crack tip, is utilized to determine the direction of subsequent crack propagation in bonded rubber cylinders. Thus, the fatigue crack in bonded rubber cylinders initiates at the point with the maximum cracking energy density, and then propagates along the direction with the lowest cracking energy density. Consequently, the curves for describing the crack propagation paths in bonded rubber cylinders with various shape factors can be obtained.

To calculate the principal stresses and resulting cracking energy density at any point of rubber, the stress distribution of a bonded rubber cylinder under axial compression should be given first. Some existing theoretical expressions based on different assumptions are employed here: the incompressibility and compressibility theories proposed by Kelly[15] and the theoretical expression derived by Horton et al.[16] For simplicity, a perfectly bonded rubber cylinder subjected to a compressive strain ε_c can be analyzed from an axisymmetrical model plotted on the r–z plane in a cylindrical coordinate system as shown in Figure 4. Some deformation assumptions are made in Kelly's incompressibility and compressibility theories: points on a vertical line in rubber lie on a parabola but horizontal planes remain horizontal when bonded rubber cylinders are subjected to a compressive strain. In addition, the resulting normal stress components at any point of rubber are approximately the same and thus treated as a hydrostatic stress state, namely $\sigma_{rr} = \sigma_{zz} = \sigma_{\theta\theta}$. As a result of the above assumptions, the stress components of rubber in a bonded rubber cylinder under axial compression obtained from Kelly's incompressibility theory are:

$$\sigma_{rr} = \sigma_{zz} = \sigma_{\theta\theta} = \frac{3G}{h^2}\left(a^2 - r^2\right)\varepsilon_c \tag{2}$$

$$\sigma_{rz} = -\frac{6G}{h^2} r\left(z - \frac{h}{2}\right)\varepsilon_c \tag{3}$$

On the other hand, the stress components of rubber obtained from Kelly's compressibility theory are:

$$\sigma_{rr} = \sigma_{zz} = \sigma_{\theta\theta} = K\left[1 - \frac{I_0(\lambda r)}{I_0(\lambda a)}\right]\varepsilon_c \tag{4}$$

$$\sigma_{rz} = -K\frac{\lambda I_1(\lambda r)}{I_0(\lambda a)}\varepsilon_c\left(z - \frac{h}{2}\right) \tag{5}$$

Herein, $\lambda = \sqrt{12G/Kh^2}$ and G and K are the shear modulus and bulk modulus of rubber, respectively. In eqs. (4) and (5), I_0 and I_1 are the modified Bessel function of first kind of order 0 and 1. Kelly's incompressibility and compressibility theories are generally employed in design to accurately evaluate the vertical stiffness of rubber bearings. However, the lateral deformation of rubber in bonded rubber cylinders under a compressive strain is not exactly a

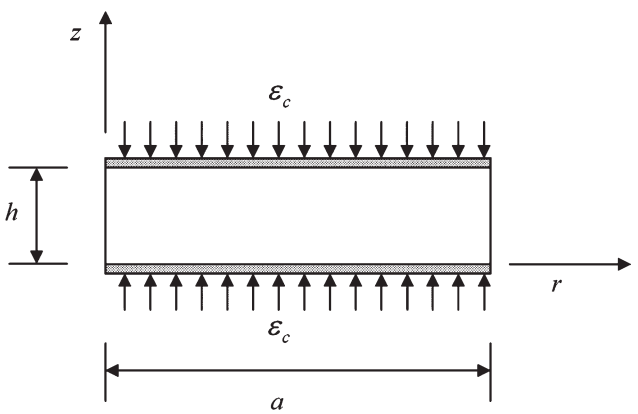

Figure 4 An axisymmetrical model on the $r - \theta - z$ plane for a bonded rubber cylinder subjected to a compressive strain ε_c.

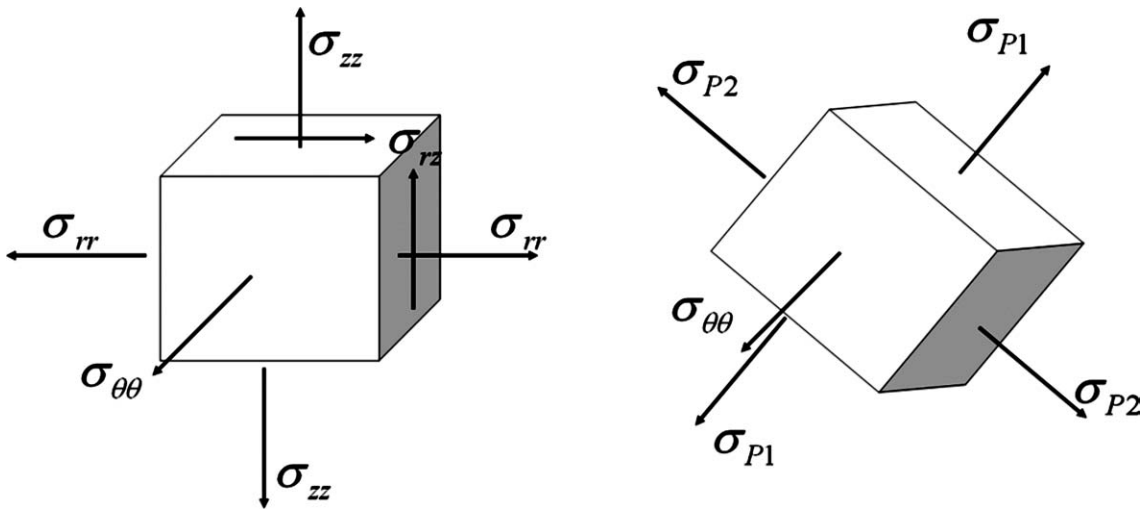

Figure 5 Stresses are transformed from cylindrical coordinate to principal coordinate on the *r*-*z* plane.

parabola as proved by Mott and Roland[17] especially for shape factors below 1. Moreover, the hydrostatic stress state assumed in Kelly's theories is inappropriate for the outermost part of bonded rubber cylinders under compression.

Without any kinematic assumption about the lateral deformation of rubber, the theoretical expressions derived by Horton et al.[16] can also be employed to determine the principal stresses and cracking energy density at any point of rubber. The stress components of rubber obtained from Horton's theory are:

$$\sigma_{rr} = \sigma_{\theta\theta} = 2\frac{F}{A}\left(1 - \frac{r^2}{a^2}\right)\frac{\cosh\left[\beta\left(z - \frac{h}{2}\right)\right]}{\cosh\frac{\beta h}{2}} \tag{6}$$

$$\sigma_{zz} = \frac{F}{A}\left\{1 + \left(1 - \frac{2r^2}{a^2}\right)\frac{\cosh\left[\beta\left(z - \frac{h}{2}\right)\right]}{\cosh\frac{\beta h}{2}}\right\} \tag{7}$$

$$\sigma_{rz} = -\frac{F\beta r}{6A}\frac{\sinh\left[\beta\left(z - \frac{h}{2}\right)\right]}{\cosh\frac{\beta h}{2}} \tag{8}$$

where $\beta = \sqrt{24/a^2}$, F is the applied force and A is the cross-sectional area of bonded rubber cylinders. The stress field derived from Horton's theory is more realistic but much complicated. It is expected that Horton's theory without any kinematic assumptions can more accurately describe the vertical stiffness and lateral deformation of rubber cylinders.

The above stress distributions derived separately from Kelly's incompressibility theory, Kelly's compressibility theory and Horton's theory are used to determine the principal stresses at any point of rubber. The transformation of the principal stresses σ_{P1} and σ_{P2} on the *r*–*z* plane is schematically illustrated in Figure 5. Furthermore, the cracking energy density due to the principal stresses σ_{P1}, σ_{P2}, and $\sigma_{\theta\theta}$ can be calculated from eq. (1), giving:

$$W_C = \frac{1}{2E}\left(\sigma_{P1}^2 - \nu\sigma_{P1}\sigma_{P2} - \nu\sigma_{P1}\sigma_{\theta\theta}\right) \tag{9}$$

where E and ν are the Young's modulus and Poisson's ratio of rubber. The distributions, contours and gradient directions of cracking energy densities in a bonded rubber cylinder with $a = 0.03$ m, $h = 0.006$ m and $S = 2.5$ under a compressive stress of 6.5 MPa obtained from Kelly's compressibility theory and Horton's theory are shown in Figures 6 and 7, respectively; the material properties of rubber are $E = 4.5$MPa and $\nu = 0.495$. It is noted that the maximum cracking energy density occurs at the outermost boundary between rubber and steel plates where the fatigue crack is most likely to initiate.

To determine the curve of crack propagation path $z = f(r)$ in rubber on the *r*–*z* plane, the decreasing rate of cracking energy density around a crack is first found:

$$\nabla W_C = \frac{\partial W_C}{\partial r}\vec{r} + \frac{\partial W_C}{\partial z}\vec{k} \tag{10}$$

where $\vec{r}$ and $\vec{k}$ are the unit vectors along the *r*-direction and the *z*-direction in a cylindrical coordinate system, respectively. The curve of crack propagation path parallel to the gradient direction of cracking energy density is thus given:

$$\frac{dr}{\partial W_C/\partial r} = \frac{dz}{\partial W_C/\partial z} \tag{11}$$

Integrating both sides of eq. (11) gives:

$$\int \frac{dr}{\partial W_C/\partial r} = \int \frac{dz}{\partial W_C/\partial z} + C \tag{12}$$

The constant C in eq. (12) can be determined from the boundary condition of crack initiation at the

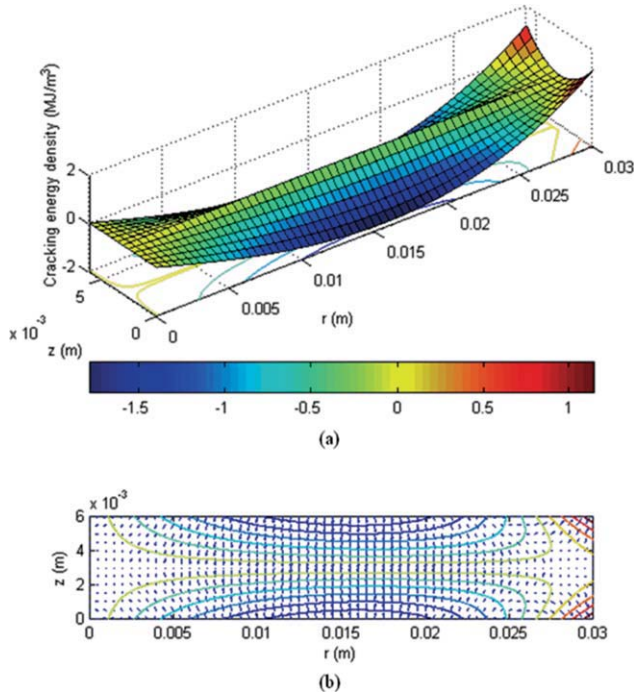

Figure 6 Computation from Kelly's compressibility theory for a bonded rubber cylinder with a shape factor $S = 2.5$ under a compressive stress 6.5 MPa. (a) The distribution of cracking energy density along the principal stress direction. (b) Contours and gradient distributions of cracking energy densities in rubber. [Color figure can be viewed in the online issue, which is available at wileyonlinelibrary.com.]

outermost boundary between rubber and steel plates with a maximum cracking energy density. Intuitively, the curve of crack propagation path in rubber $z = f(r)$ can be obtained directly. However, the expressions for describing the principal stresses σ_{P1} and σ_{P2} and cracking energy density W_C at any point of rubber derived from the aforementioned three theories are very complicated. As a result, no analytical solution of $z = f(r)$ is possible to obtain through the uses of eqs. (10)–(12). Alternatively, a linear extrapolation technique is employed to numerically determine the curves of crack propagation path in bonded rubber cylinders with various shape factors.

FINITE ELEMENT NUMERICAL ANALYSIS

A finite element package ABAQUS was employed to compute the stress distributions and resulting cracking energy densities in bonded rubber cylinders with various shape factors under compression. The radius and height of the cylinders were $a = 0.03$ m and $h = 0.15$, 0.015, 0.006, and 0.0015 m corresponding to shape factors of $S = 0.1$, 1.0, 2.5, and 10, respectively. Because of the symmetries of geometry and loading configuration, a half height model of bonded rubber cylinders was first meshed in finite element numerical analyses. The elastic properties of rubber were set to be $E = 4.5$MPa and $\nu = 0.495$. Figure 8 shows the undeformed FEA mesh and boundary conditions of a bonded rubber cylinder with a shape factor $S = 2.5$. In running finite element numerical analyses, CAX3 (three-noded linear axisymmetrical triangle) elements were used when the simulation of crack propagation and the generation of mesh are of concern. Since steel plates are much stiffer than rubber and they are perfectly bonded to each other in rubber bearings, some appropriate boundary conditions were prescribed in finite element numerical analyses. The x-direction displacement u_x and the rotation r_{xy} on the bottom edge of the half height numerical model of bonded rubber cylinders were set to be zero while $u_x = r_{xy} = 0$ but $u_x \neq 0$ were prescribed on its upper edge. The mesh near the outermost boundary between rubber and steel plate, where fatigue crack initiation occurs most likely, was much finer. A compressive strain $\varepsilon_c = 0.01$ was imposed on the bottom side of the half height numerical model by prescribing a boundary condition of y-direction displacement $u_y = \varepsilon_c h/2$. The un-deformed and deformed meshes

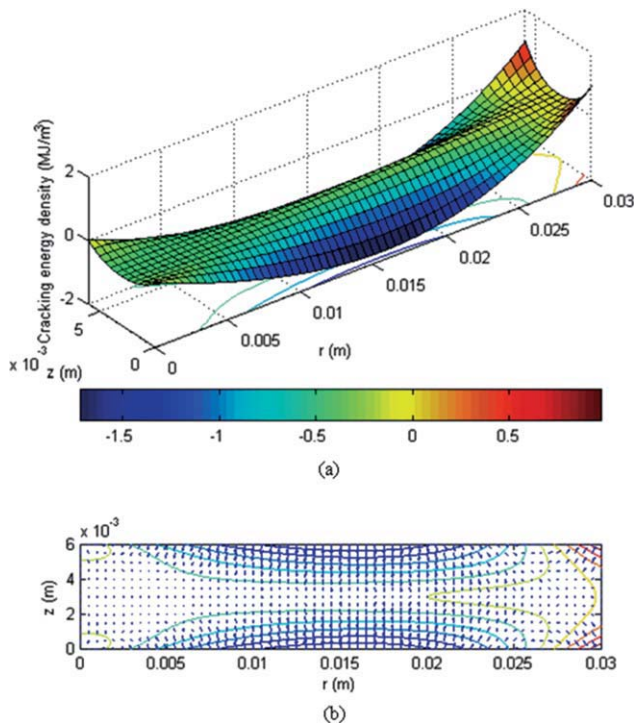

Figure 7 Computation from Horton's theory for a bonded rubber cylinder with a shape factor $S = 2.5$ under a compressive stress 6.5 MPa. (a) The distribution of cracking energy density along the principal stress direction. (b) Contours and gradient distributions of cracking energy densities in rubber. [Color figure can be viewed in the online issue, which is available at wileyonlinelibrary.com.]

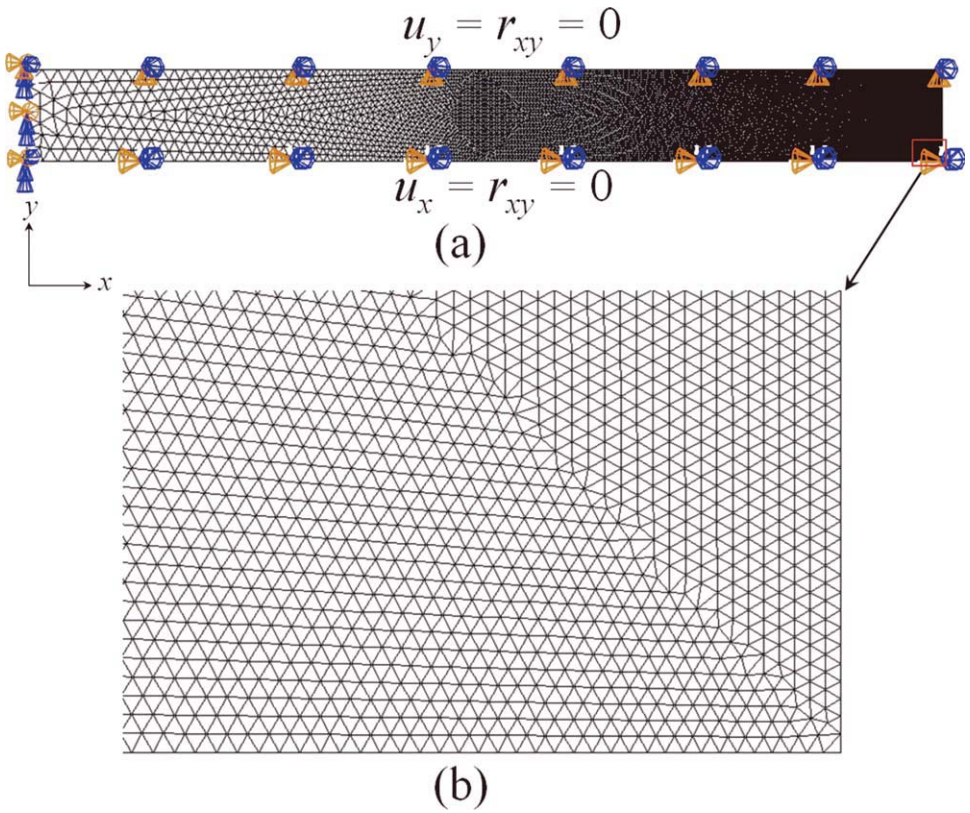

Figure 8 (a) The undeformed mesh and boundary conditions, and (b) the partially enlarged mesh for finite element analyses of a bonded rubber cylinder with a radius $R = 0.03$ m and a height $h = 0.006$ m and a shape factor $S = 2.5$. [Color figure can be viewed in the online issue, which is available at wileyonlinelibrary.com.]

of the half height finite element numerical models are shown in Figures 8 and 9, respectively.

When the FEA numerical model without any preexisting crack was subjected to a compressive strain, the principal stresses at each node were first computed and then used to calculate its cracking energy density from eq. (9). It was assumed that the fatigue crack initiates at a node with the maximum cracking energy density. Meanwhile, the crack propagation in the FEA numerical model was assumed to be along the direction passing through a nearest neighboring node around a crack tip with the lowest cracking energy density. Record the coordinate of the nearby node with the lowest cracking energy density and then rebuild a similar FEA numerical model including a new crack surface extending from the point of crack initiation to the next crack tip where the node with the lowest W_C found previously. The new crack was made by adding some nodes very close but different to the original ones along the crack surface to create a crack opening surface and sharing the same node at the crack tip. The contact properties of the two opposite sides of a crack surface in running finite element package ABAQUS were set to be hard contact and frictionless to prevent them from overlapping each other when the half height numerical model was under compression. A compressive strain $\varepsilon_c = 0.01$ was again imposed on the rebuilt FEA numerical model with an extended crack and then the principal stresses and resulting cracking energy density at each node around the new crack tip were computed to decide the direction of subsequent crack propagation. By repeating the above steps, the curve of crack propagation path in the FEA numerical model can thus be numerically determined. The simulation of a fatigue crack in a bonded rubber cylinder with a radius $a = 0.03$ m, a height $h = 0.006$ m and a shape factor $S = 2.5$ is shown in Figure 10.

At the same time, CAX4 (four-noded bilinear axisymmetric quadrilateral) elements and two different degrees of freedom of mesh configuration were used for a bonded rubber cylinder with a shape factor $S = 2.5$ to evaluate the effects of element type and mesh fineness on the FEA numerical results of crack propagation. The mesh configurations of FEA numerical model with CAX4 elements and two different degrees of freedom are shown in Figure 11.

RESULTS AND DISCUSSION

On the basis of Kelly's incompressibility theory, Kelly's compressibility theory with $\nu = 0.495$ and Horton's theory, the theoretical results for describing the crack propagation paths in bonded rubber

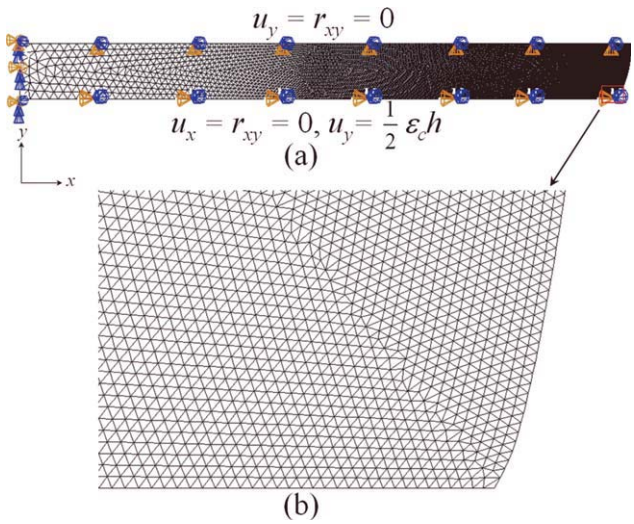

Figure 9 (a) The deformed mesh and boundary conditions, and (b) the partially enlarged mesh for finite element analyses of a bonded rubber cylinder with a radius $R = 0.03$ m and a height $h = 0.006$ m and a shape factor $S = 2.5$. [Color figure can be viewed in the online issue, which is available at wileyonlinelibrary.com.]

cylinders with a radius of $a = 0.03\ m$, a height of $h = 0.15$, 0.015, 0.006, and 0.0015 m separately corresponding to a shape factor of $S = 0.1$, 1, 2.5, and 10 are shown in Figure 12(a–c), respectively. It is noted that the curves of crack propagation paths obtained from quasi-statically theoretical analyses are independent on the magnitude of external force we imposed. From Figure 12, it is seen that the extent of crack propagation in rubber decreases consistently with increasing shape factor of bonded rubber cylinders. The reason for that is because the region of principal tensile stresses and resulting cracking energy density in bonded rubber cylinders with larger shape factors are smaller than those with smaller shaper factors when they are subjected to a compressive strain. Therefore, it can be said that the shape factor of a circular rubber bearing is a decisive factor in determining the curve of crack propagation path. The maximum principal tensile stress in circular rubber bearings with larger shape factors decreases and the region of principal tensile stresses is also reduced, leading to an increase of their fatigue resistance.

In addition, the slopes of the curves of crack propagation paths in bonded rubber cylinders with larger shape factors under compression are apparently different from those with smaller shape factors due to the variation of their stress field. It is also noted that the curves of crack propagation paths in bonded rubber cylinders with a smaller shape factor of $S = 0.1$ derived from both Kelly's incompressibility and compressibility theories deviate substantially from those with larger shape factors. The above finding

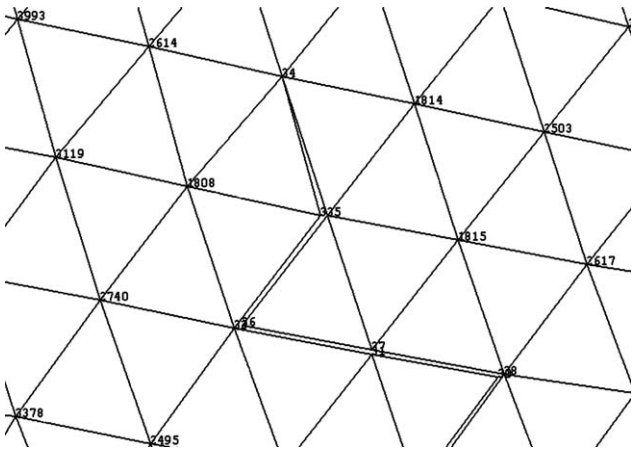

Figure 10 The fatigue crack simulated in finite element analyses for a bonded rubber cylinder with a radius $R = 0.03$ m and a height $h = 0.006$ m and a shape factor $S = 2.5$.

can be attributed to the assumption of parabolic lateral deformation in both Kelly's incompressibility and compressibility theories which has been verified to be invalid for the case of smaller shape factor.[17]

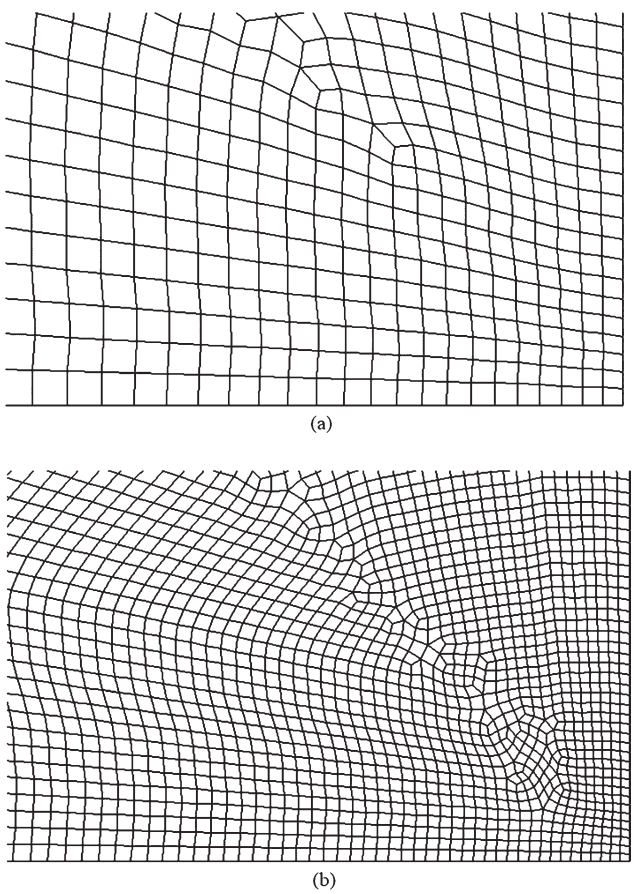

Figure 11 The enlarged mesh of CAX4 elements with different degrees of freedom in finite element analyses for a bonded rubber cylinder with a radius $R = 0.03$ m and a height $h = 0.006$ m and a shape factor $S = 2.5$, (a) 35,100 degrees of freedom and (b) 63,800 degrees of freedom.

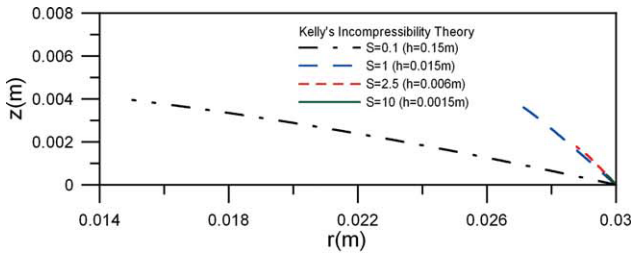

(a) Kelly's incompressibility theory

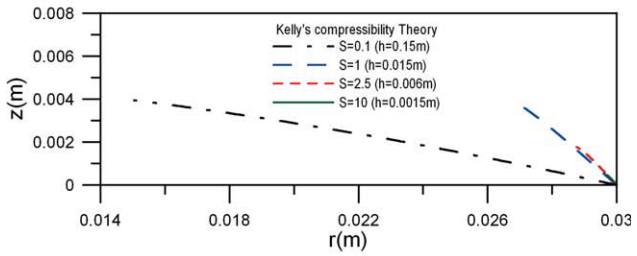

(b) Kelly's compressibility theory

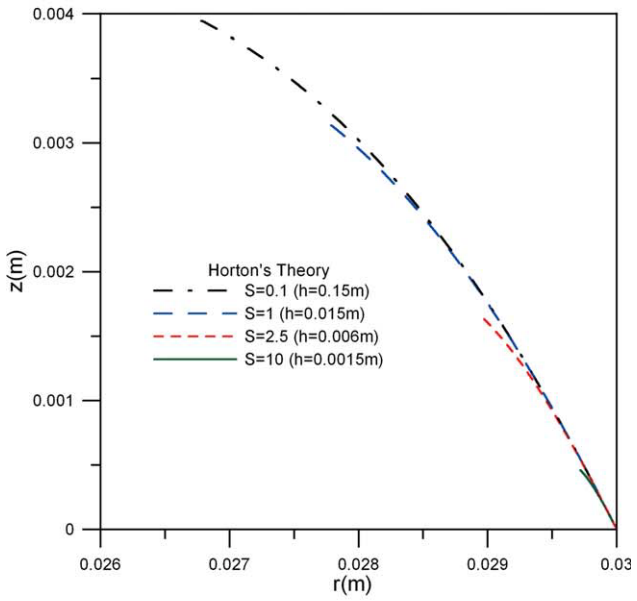

(c) Horton's theory

Figure 12 The curves of crack propagation paths in bonded rubber cylinders with different shape factors S = 0.1, 1.0, 2.5, and 10 obtained from (a) Kelly's incompressibility theory, (b) Kelly's compressibility theory, (c) Horton's theory. [Color figure can be viewed in the online issue, which is available at wileyonlinelibrary.com.]

On the contrary, the curves of crack propagation paths in bonded rubber cylinders derived from Horton's theory coincide with each other, regardless of their shape factor. Hence, it can be said that Horton's theory provides more accurate stress distribution in bonded rubber cylinders under axial compression and can be appropriately employed for the prediction of the curves of crack propagation paths.

The curves of crack propagation paths in bonded rubber cylinders obtained individually from finite element numerical analyses, Kelly's incompressibility theory, Kelly's compressibility theory and Horton's theory are plotted in Figures 13–16 for different shape factors S = 0.1, 1, 2.5, and 10, respectively. In Figures 13–16, the FEA numerical results of crack propagation in bonded rubber cylinders with any

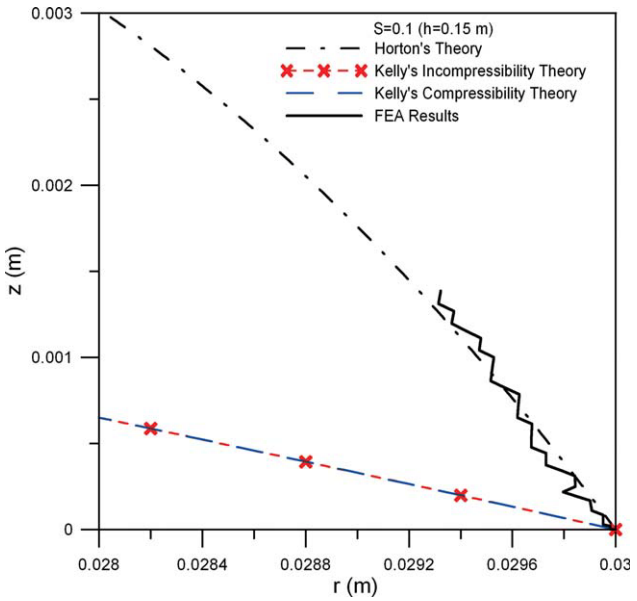

Figure 13 The curves of crack propagation paths in a bonded rubber cylinder with a shape factors S = 0.1 obtained separately from Kelly's incompressibility theory, Kelly's compressibility theory, Horton's theory, and FEA results. [Color figure can be viewed in the online issue, which is available at wileyonlinelibrary.com.]

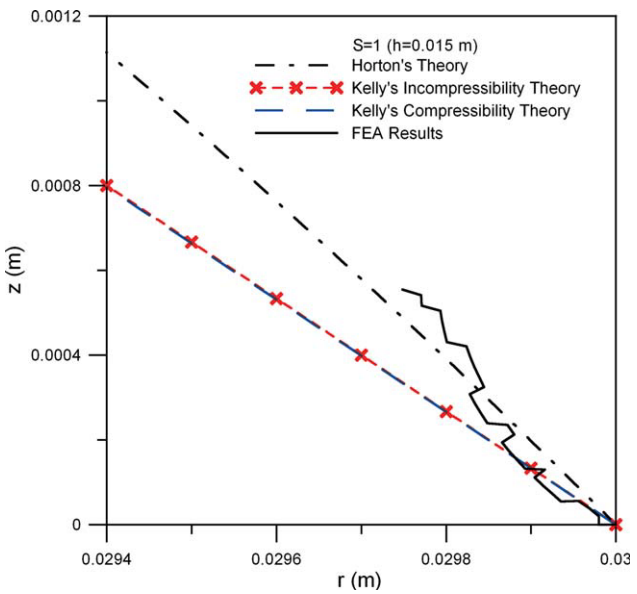

Figure 14 The curves of crack propagation paths in a bonded rubber cylinder with a shape factors S = 1 obtained separately from Kelly's incompressibility theory, Kelly's compressibility theory, Horton's theory, and FEA results. [Color figure can be viewed in the online issue, which is available at wileyonlinelibrary.com.]

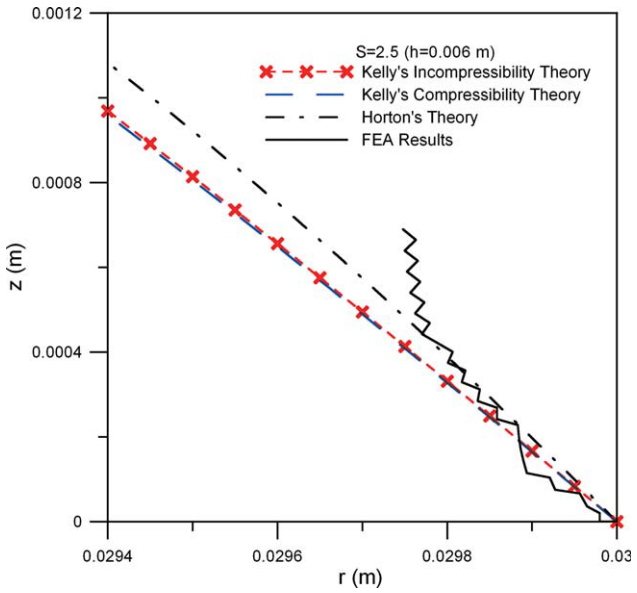

Figure 15 The curves of crack propagation paths in a bonded rubber cylinder with a shape factors $S = 2.5$ obtained separately from Kelly's incompressibility theory, Kelly's compressibility theory, Horton's theory, and FEA results. [Color figure can be viewed in the online issue, which is available at wileyonlinelibrary.com.]

shape factor were obtained by rebuilding mesh of the half height numerical model and extending crack length in rubber repeatedly for fifty times. It is found that the theoretical results derived from Kelly's incompressibility and compressibility theories are gradually close to those derived from Horton's theory as the shape factor increases. But, the theoretical results derived from Horton's theory are much closer to the FEA numerical results for bonded rubber cylinders with a smaller shape factor $S = 0.1$. Again, it is found that Kelly's theories are not suitable for predicting the curves of crack propagation paths in circular rubber bearings with a smaller shape factor such as $S = 0.1$ in the study.

In Figures 13–16, the FEA numerical results also indicate that the fatigue crack initiates at the point near the outermost boundary between rubber and steel plates and then propagates inwards to the center of a bonded rubber cylinder. It should be noted that although the direction of crack propagation at each step in running finite element analysis is dependent on the mesh of the half height numerical model, the resulting curve of crack propagation path is approximately the same to some extent. Meanwhile, the curves of crack propagation paths simulated from finite element numerical analyses become slightly steeper after the fatigue cracks extend to some certain lengths as compared to those obtained from the three theoretical models. The above finding from finite element numerical analyses is confirmed by a similar observation reported by Lindley and Stevenson.[2] The difference between theoretical and FEA numerical results can be attributed to the assumption of undisturbed stress distribution in bonded rubber cylinders we proposed. In other words, the stress distributions derived from Kelly's incompressibility, Kelly's compressibility and Horton's theories are no longer appropriate especially when the cracks extend to some certain lengths.

Finally, the experimental observations[1] on the saw-cut cross sections of specimens as shown in Figure 1 are also presented in Figure 17 and then compared with the theoretical results of crack propagation derived from Horton's theory, and the FEA numerical results from the half height model with two different element types (CAX3 elements and CAX4 elements) and degrees of freedom (35,100 and 63,800), respectively. From the figure, it is seen clearly that fatigue cracks initiate at the outermost boundary between rubber and steel plates and then propagate inwards to the center of rubber bearings. The theoretical and numerical results on the fatigue crack initiation and propagation provided here ascertain the experimental observation on the saw-cut cross section of rubber bearings under cyclic compression reported previously. On the other hand, the FEA numerical results of the half height model with different element type and degrees of freedom are close to the curves of crack propagation paths theoretically determined from Horton's theory. Therefore, Horton's theory can be employed to calculate the cracking energy density and to predict the

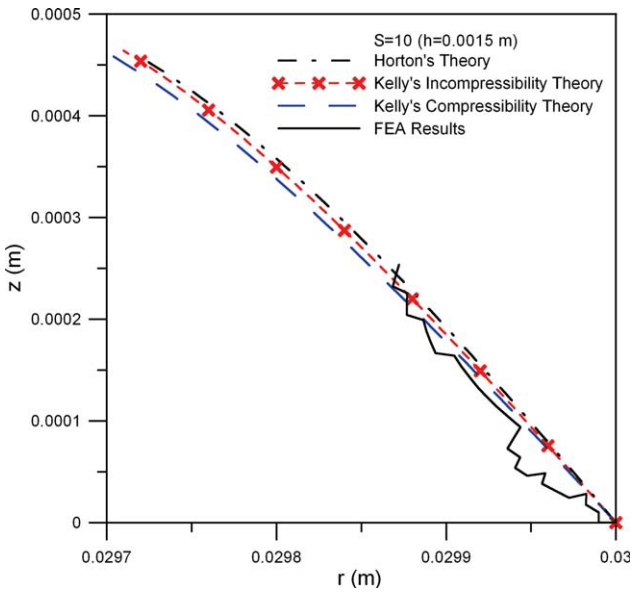

Figure 16 The curves of crack propagation paths in a bonded rubber cylinder with a shape factors $S = 10$ obtained separately from Kelly's incompressibility theory, Kelly's compressibility theory, Horton's theory, and FEA results. [Color figure can be viewed in the online issue, which is available at wileyonlinelibrary.com.]

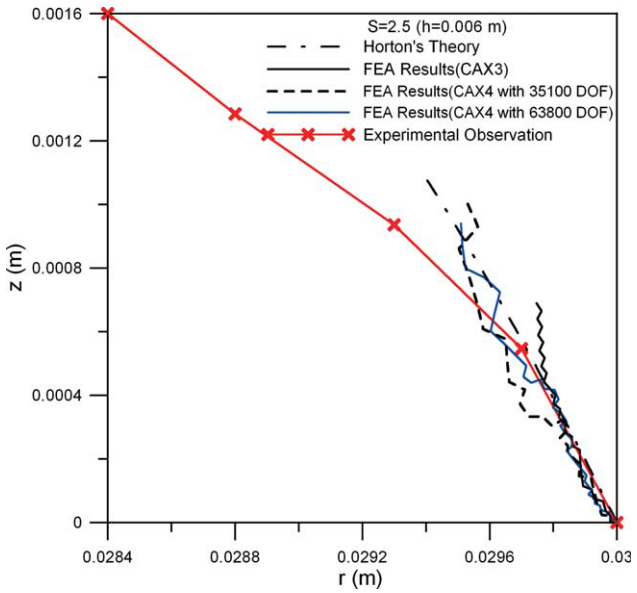

Figure 17 The curves of crack propagation paths in a bonded rubber cylinder with a shape factors $S = 2.5$ obtained individually from Horton's theory, FEA results with CAX3 elements and CAX4 elements and two different degrees of freedom and experimental observation in Figure 1. [Color figure can be viewed in the online issue, which is available at wileyonlinelibrary.com.]

fatigue crack initiation and propagation for circular rubber bearings with various shape factors.

CONCLUSIONS

The stress distributions in bonded rubber cylinders derived individually from Kelly's incompressibility theory, Kelly's compressibility theory and Horton's theory were utilized to calculate the maximum principal tensile stress and resulting cracking energy density at any point in rubber. Fatigue crack initiation occurs at the point with the maximum cracking energy density while crack propagation is along the direction with the lowest cracking energy density. It is found that fatigue cracks initiate at the outermost boundary between rubber and steel plates and then propagate inwards along a direction depending on the shape factor of bonded rubber cylinders. At the same time, quasi-static finite element numerical analyses to simulate the fatigue crack initiation and propagation in bonded rubber cylinders were conducted. It is found that the extent of crack propagation decreases with increasing shape factor. Hence, circular rubber bearings with a larger shape factor have a better fatigue resistance. Meanwhile, the curves of crack propagation paths obtained from finite element numerical analyses become slightly steeper when fatigue cracks extend to some certain lengths. In addition, it is verified that the stress distribution derived from Horton's theory is more suitable to calculate the cracking energy density and to predict the fatigue crack initiation and propagation for circular rubber bearings with various shape factors.

References

1. Chou, H. W.; Huang, J. S. J Appl Polym Sci 2008, 107, 1635.
2. Lindley, P. B.; Stevenson, A. Rubber Chem Technol 1982, 55, 337.
3. Leicht, D. C.; Yeoh, O. H.; Gent, A. N.; Padovan, J.; Mullen, R. L. Rubber Chem Technol 2003, 76, 160.
4. Leicht, D. C.; Rimnac, C.; Mullen, R. L. Rubber Chem Technol 2003, 76, 365.
5. Mars, W. V. Tire Sci Technol 2001, 29, 171.
6. Mars, W. V. Rubber Chem Technol 2002, 75, 1.
7. Dizon, E. S.; Hicks, A. E.; Chirco, V. E. Rubber Chem Technol 1974, 47, 231.
8. Roland, C. M.; Smith, C. R. Rubber Chem Technol 1985, 58, 806.
9. Hamed, G. Rubber Chem Technol 1994, 67, 529.
10. Mars, W. V.; Fatemi, A. Int J Fatigue 2002, 24, 949.
11. Lake, G. J.; Lindley, P. B. J Appl Polym Sci 1966, 10, 343.
12. Choi, I. S.; Roland, C. M. Rubber Chem Technol 1996, 69, 591.
13. Chou, H. W.; Huang, J. S.; Lin, S. T J Appl Polym Sci 2007, 103, 1244.
14. Gdoutos, E. E. Fracture Mechanics—An Introduction; Kluwer Academic Publishers: Dordrecht, 1993; Chapter 7.
15. Kelly, J. M. Earthquake-Resistant Design with Rubber. Springer-Verlag: London, 1993.
16. Horton, J. M.; Tupholme, G. E.; Gover, M. J. C. J Appl Mech 2002, 69, 836.
17. Mott, P. H.; Roland, C. M. Rubber Chem Technol 1995, 68, 739.